Dalton Transactions

RSC Publishing

PAPER

View Article Online
View Journal | View Issue

Cite this: *Dalton Trans.*, 2013, **42**, 6879

Insights into the dielectric and luminescent properties of $Na_{0.5}Pr_{0.003}Bi_{0.497-x}La_xTiO_3$ synthesized by the Pechini method

Rigoberto López-Juárez,*[a] R. Castañeda-Guzmán,[a] Fernando Rubio-Marcos,[b] M. E. Villafuerte-Castrejón,[c] Enrique Barrera-Calva[d] and Federico González*[d]

Received 5th December 2012,
Accepted 17th February 2013

DOI: 10.1039/c3dt32911a

www.rsc.org/dalton

Lead-free ferroelectric ceramics based on the $Na_{0.5}Bi_{0.5}TiO_3$ system, in solid solution with Pr^{3+} and La^{3+}, are synthesized by the Pechini method at low temperature. The powders calcined at 700 °C are found to be below 200 nm in mean crystal size. The dielectric properties reveal a diffuse phase transition. In $Na_{0.5}Bi_{0.5}TiO_3$ ceramics the rhombohedral to tetragonal transition temperature (T_{R-T}) appears near 190 °C, and the Curie temperature (T_C) at 280 °C. These transitions are shifted when Pr^{3+} and La^{3+} cations are introduced into the lattice. The ferroelectric properties are also affected, causing the remnant polarization and coercive field to diminish with the increase in La^{3+} content. In addition, the piezoelectric properties decrease in the same way with La^{3+} concentration. Finally, the red luminescence of Pr^{3+} is improved when lanthanum concentration is increased.

Introduction

Lead-free ferroelectric ceramics are currently under intense investigation due to the need to replace $PbTi_{1-x}Zr_xO_3$ (PZT) materials. Some of the most interesting solid solutions are $K_{0.5}Na_{0.5}NbO_3$ (KNN), $Ba_{1-x}Ca_xTi_{1-y}Zr_yO_3$ (BCTZ) and $Na_{0.5}Bi_{0.5}TiO_3$ (NBT).[1–3] NBT has high P_r (~38 μC cm^{-2})[4] and it is believed to have rhombohedral structure with space group *R*3*c*. Nevertheless, there is a controversy about its structure at room temperature.[5,6] Looking at the crystal structure adopted by NBT between 200 and 320 °C, there is a discrepancy. Some authors have reported a tetragonal ferroelectric lattice[5] while others assumed it is antiferroelectric based on the ferroelectric loops measured at high temperature.[7] Despite the crystalline structure adopted by the NBT at 200–320 °C, the piezoelectric properties decrease abruptly at the phase transition. Concerning the ferroelectric and piezoelectric properties, NBT presents high conductivity and dielectric losses because of the high vacancy concentration produced during the sintering process at high temperature. The conventional solid state reaction used for the synthesis of NBT demands calcinations at ~900 °C and sintering at 1200 °C that promotes such vacancies. In order to reduce the temperature of the synthesis and increase the electrical resistivity during the poling process, chemical methods can be used to produce nanometric powders, namely, sol–gel and hydrothermal methods are effective routes to obtain NBT pure phase.[8,9]

In addition to the piezoelectric and ferroelectric applications of NBT, today it is being considered as a host material for lanthanide doping for luminescent applications.[10,11] For this purpose, Pr^{3+} doping has very attractive properties, producing red emission under ultraviolet light illumination, in addition to that produced by exciting through the f–f levels in the visible region. As a consequence, co-doping by suitable elements to minimize the temperature sensitivity, reduce the dielectric losses in the modified NBT system, and enhance the luminescent applications is a very active research field. Nevertheless, there are still some structural, electrical and optical aspects that remain controversial with respect to the role of dopants in this system.

In this work, La^{3+}/Pr^{3+} cations were chosen to act as the co-dopant and, therefore, the aim of this work will be the study of the relationship between the crystalline symmetry, the ferro–piezoelectric and the luminescent properties in the co-doped NBT system. And to accomplish this goal, the $Na_{0.5}Bi_{0.5}TiO_3$ and $Na_{0.5}Pr_{0.003}Bi_{0.497-x}La_xTiO_3$ ($0 \leq x \leq 0.05$) ceramics are synthesized by the Pechini method.

[a]*Centro de Ciencias Aplicadas y Desarrollo Tecnológico, Universidad Nacional Autónoma de México, A.P. 70-186, Coyoacán, México D.F., Mexico. E-mail: rigobertolj@yahoo.com.mx; Fax: +52 55 56 16 13 71; Tel: +52 55 56 22 46 41x24646*

[b]*Departamento de Electrocerámicas, Instituto de Cerámica y Vidrio, CSIC, Kelsen 5, 28049 Madrid, Spain*

[c]*Instituto de Investigaciones en Materiales, Universidad Nacional Autónoma de México, Circuito Exterior S/N, A.P. 70-360, México D.F., Mexico*

[d]*Departamento de Ingeniería de Procesos e Hidráulica, Universidad Autónoma Metropolitana-Iztapalapa, A.P. 55-534, 09340 México D.F., Mexico. E-mail: fgg@xanum.uam.mx*

Experimental

Synthesis and sintering of powders

In this work the Pechini method was used for the preparation of $Na_{0.5}Pr_{0.003}Bi_{0.497-x}La_xTiO_3$ (NPBLT) ceramics ($0 \leq x \leq 0.05$), also the $Na_{0.5}Bi_{0.5}TiO_3$ (NBT) composition was obtained as a reference. This method involves the preparation of a polymeric resin from organic acids, alcohols and the ions required for the desired material. Both, the acid and alcohol must be poly-functional compounds for preparing a desirable three-dimensional polymeric network.[12–14]

The raw materials used were sodium acetate trihydrate (99%), bismuth nitrate pentahydrate (98%), praseodymium nitrate hexahydrate (99.9%), titanium isopropoxide (97%), citric acid, ethylene glycol and absolute ethanol. In a typical synthesis, the titanium isopropoxide was dissolved in absolute ethanol under continuous stirring, and then citric acid was immediately added for stabilization of the titanium ion. After that, sodium acetate, praseodymium nitrate, bismuth nitrate, lanthanum nitrate and ethylene glycol were added. The solution was kept at 60 °C for 8 hours for complete dissolution of sodium acetate and bismuth nitrate. Later, the temperature was further raised to 75 °C for evaporation of the excess alcohol resulting in a viscous yellowish solution. For promoting polymerization the temperature was set at 90 °C. The resin was then transferred to an oven for a heat treatment at 300 °C for 30 min. Then, the pre-calcined powders were heat treated at 700 °C for 1 h. The calcined powders were cold-isostatically pressed at 200 MPa into disks of 10 mm diameter and 0.7 mm thickness. The pellets were finally sintered in air at 1100 °C for 2 h.

Structural, dielectric and ferroelectric characterization

The powders and sintered specimens were structurally characterized by X-ray diffraction (Bruker D8 Advance Cu $K_{\alpha 1}$ 1.5406), the morphology was observed by scanning electron microscopy (JEOL7600F). Electrical characterization was carried out on ceramic discs. A silver slurry was coated on both sides of the discs and then treated at 700 °C as electrodes. The temperature dependence of permittivity was measured using an impedance analyzer (HP4294A, Agilent) in the frequency range of 1 kHz–1000 kHz and the temperature range of 30–500 °C, using a heating rate of 2 °C min^{-1}. Ferroelectric hysteresis loops were recorded in the temperature range of 25–250 °C using a hysteresis meter (RT 6000 HVS, RADIANT Technologies).

Piezoelectric characterization

The piezoelectric properties were evaluated, after a classical poling process. This was carried out in a silicone oil bath at temperatures between 100–125 °C under a DC electric field of 30 kV cm^{-1} for 30 min. The piezoelectric constant d_{33} was measured using a piezo-d_{33} meter (YE2730A d_{33} METER, APC International) in the temperature range of 25–300 °C.

Luminescence characterization

The emission and excitation spectra, and the luminescence decay curves were recorded with an Edinburgh Instruments FSP920 spectrofluorometer based on the method of single photon counting which combines steady state and phosphorescence lifetime measurements. In the latter the electronics operate in multichannel scaling mode. The spectrofluorometer is equipped with a 450 W xenon lamp as a CW light source and an R928P PMT as a detector. In order to avoid the light dispersion, a double monochromator (two coupled 0.3 m) was employed to excite the samples. The emission was detected using a 0.3 m monochromator. All the excitation and emission spectra were corrected for the wavelength dependent responses of the Xe lamp and the detector, respectively. For the measurements of luminescence decay, the excitation photons were provided by a 60 W μF920H pulsed Xe flashlamp with a pulse width of ~1.5 μs and a repetition rate of 100 Hz. The absorption spectra were obtained by using the diffuse reflectance technique. The measurements were performed in a Cary 5 spectrophotometer equipped with a Praying Mantis (Harrick Scientific Products, Inc.) accessory for diffuse reflection spectroscopy. The spectra were recorded in the wavelength range between 250 and 700 nm.

Results and discussion

The XRD results for NBT and NPBLT calcined powders are shown in Fig. 1. The pure perovskite phase is observed for all compositions. This is possible due to the mixing of the reagents at atomic level achieved by the Pechini method. It is well-known that the polymerization aids the homogeneous distribution of cations,[12,13] lowering the required energy for the crystallization. Furthermore, the low temperature crystallization allows the preparation of nanocrystalline powders. Also in

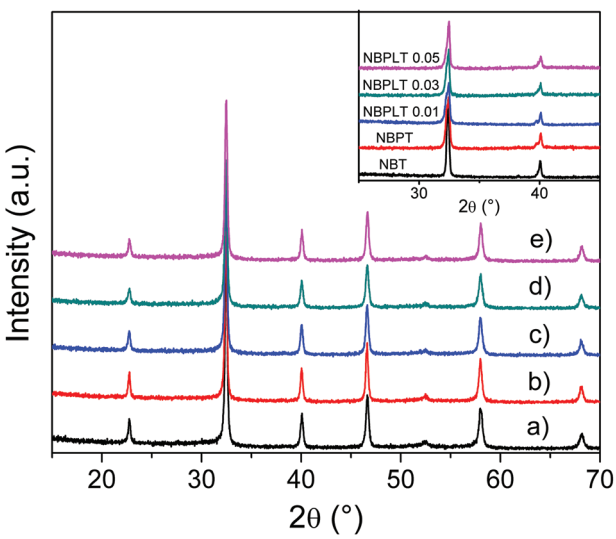

Fig. 1 XRD of calcined powders at 700 °C, (a) NBT, (b) NPBT; NPBLT, (c) x = 0.01, (d) x = 0.03 and (e) x = 0.05 (where x refers to La^{3+} doping).

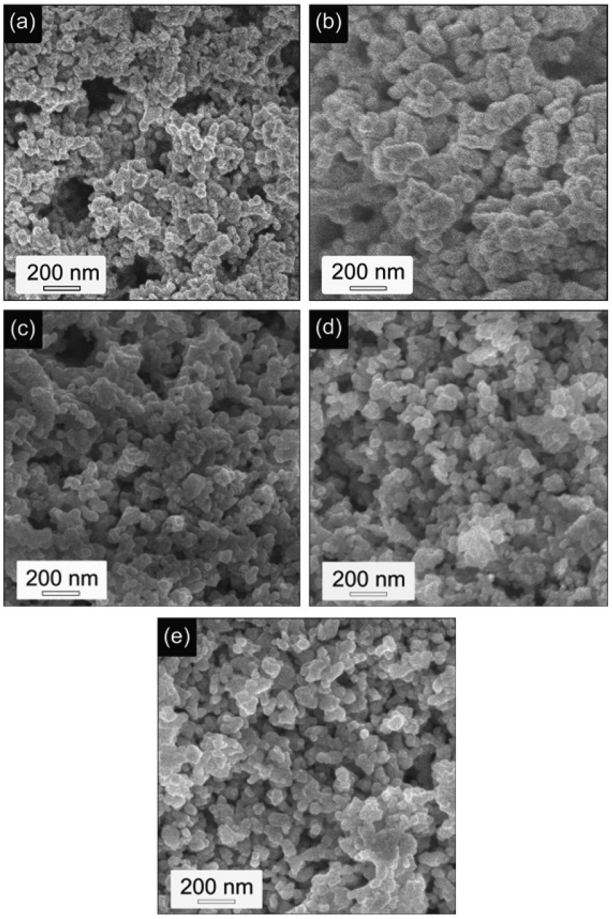

Fig. 2 SEM pictures of NBT powders calcined at 700 °C for 1 h, (a) NBT, (b) NPBT; NPBLT, (c) $x = 0.01$, (d) $x = 0.03$ and (e) $x = 0.05$.

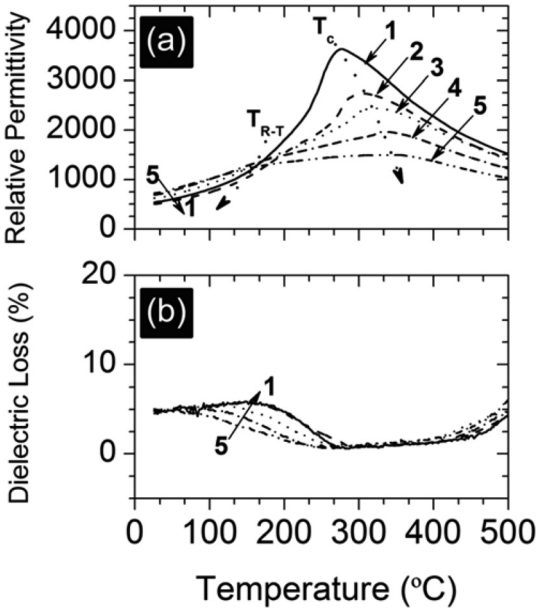

Fig. 3 (a) The temperature dependence of the relative permittivity and (b) dielectric loss (tan δ) for NBT, NPBT and NPBLT ceramics (at 100 kHz). The ceramic compositions represented in (a–b) are the following: (**1**) $Na_{0.5}Bi_{0.5}TiO_3$; (**2**) $Na_{0.5}Pr_{0.003}Bi_{0.497}TiO_3$; (**3**) $Na_{0.5}Pr_{0.003}Bi_{0.487}La_{0.01}TiO_3$; (**4**) $Na_{0.5}Bi_{0.467}Pr_{0.03}$-$La_{0.03}TiO_3$; (**5**) $Na_{0.5}Bi_{0.447}Pr_{0.03}La_{0.05}TiO_3$. The dotted arrows marked in (a) correspond to the T_{R-T} and T_C evolution.

Fig. 1 (the inset) the XRD patterns of sintered pellets are shown, where it can be observed that no secondary phases are present.

In Fig. 2 the SEM images of calcined powders are shown. The mean crystal size measured in NBT powders is 75 nm. Fine powders are a prerequisite for obtaining high density sintered materials. Lead-free piezoceramics present the drawback of the high volatility of bismuth and alkaline elements. This, unavoidably produces cation and oxygen vacancies within the lattice. The poling process is sometimes difficult because of the increased ionic conductivity. Moreover, the NBT ceramics have a high coercive field; this would even reinforce the difficulty in poling. Then, the low crystallization temperature reduces the creation of vacancies and enhances the polarization process of ceramics.[6]

The permittivity (ε') and dielectric losses (tan δ) *versus* temperature graphs are shown in Fig. 3(a–b). It can be seen that two anomalies exist in the permittivity for NBT, marked as point **1** in Fig. 3(a). One is near 190 °C and the other at 280 °C, these are assigned to the rhombohedral–tetragonal transition temperature (T_{R-T}) and the Curie temperature (T_C), respectively. These temperatures are a little different from those reported before.[7] One reason for the discrepancy is the processing method used by the other authors who used the solid state reaction. Then, the amount of vacancies affects the temperature at which these transitions appear, the values obtained in this work are close to those reported previously. When Pr^{3+} is added (composition marked as point **2** in Fig. 3a), the permittivity magnitude decreases at T_C, and it is shifted to 300 °C. A slight decrease of the rhombohedral–tetragonal transition temperature (T_{R-T}) is also detected with the Pr^{3+} addition, close to ~175 °C. The Pr^{3+} ion enters the A site of the perovskite structure. It is known that in PZT[15] the interaction of lead with oxygen affects the lattice and then the piezoelectric properties. It seems that Pr^{3+} has a considerable effect on the lattice, modifying T_C, T_{R-T} and the magnitude of ε'.

When lanthanum is introduced into the A-site positions of the perovskite lattice, ε' and T_C are affected further (compositions marked as points **3–5** in Fig. 3a). ε' decreases from 2500 to 1500 when the La^{3+} content increases from 1 to 5 at% and T_C is shifted from ~320 to ~350 °C. On the other hand, T_{R-T} shifts to lower values, from ~150 °C at 1 at% to near room temperature at 5 at%, *i.e.* the stability range of the tetragonal phase has increased.

The dielectric losses are also shown in Fig. 3(b). It is shown that tan δ remains close to 5% for all compositions at room temperature but when T_{R-T} is reached tan δ decreases and after T_C, it increases again. It is also evident that only when the temperature is well above T_C, the dielectric losses increase rapidly.

Concerning the nature of T_{R-T}, recently,[7] some evidence was found based on the ferroelectric loops measured at high

temperature. Nonetheless, the loops were acquired at just three temperatures and the transitions are not clearly seen. For this purpose, the ferroelectric loops were measured at several temperatures for the different solid solutions.

The loops for the NBT at room temperature are not saturated and are similar to those of a normal dielectric ceramic (see Fig. 4a at 25 °C). This is because the high voltage source used in this work is just 4 kV and it cannot achieve the coercive field of NBT (7.3 kV mm^{-1}).[16] On increasing the temperature, the loops become saturated due to the easy switching of domains. At 125 °C the loops are well-saturated; $2P_r$ is near 44 μC cm^{-2} and $2E_C$ close to 54 kV cm^{-1}. A further increase in temperature makes the loops slim, and at 200 °C an anomaly is perceptible, which corresponds to the T_{R-T} phase transition. Most important, at 225 °C the double hysteresis loops are clearly seen, confirming the existence of an antiferroelectric phase. Some authors explain that this behavior is due to the existence of orthorhombic phase regions within the rhombohedral one[17] called "modulated phase". These results also confirm the phase transition observed in the permittivity analysis.

The influence of Pr^{3+} in the ferroelectric loops is also evident (see Fig. 4b). Similar to the NBT ceramics, the loops are only saturated at temperatures higher than 100 °C. In this case, the antiferroelectric phase appears at lower temperatures, as confirmed by the dielectric permittivity.

In the sample with 0.01 La^{3+} content, the antiferroelectric phase begins to appear at 150 °C as measured by ε', Fig. 4(c–d). The coercive field is diminished but P_r remains almost constant. Then, it could be concluded that La^{3+} has enhanced the ferroelectric properties of NBT. On further increasing La^{3+}, T_{R-T} appears at even lower temperatures (125 °C with 3 at% La^{3+}) and finally the NBT becomes pseudocubic, with the ferroelectric loops similar to a normal dielectric material (at 0.05).

Summarizing the ferroelectric behavior, Fig. 4(e) shows the evolution of $2P_r$ on NBT, NPBT and NPBLT systems as a function of the temperature. From Fig. 4(e) it can be observed that the ferroelectric/antiferroelectric behavior depends on the La^{3+} content; for each composition, T_{R-T} decreases with the doping concentration. In addition, the P_r evolution allows determining the optimal temperature for the poling process which depends on the composition.

Taking into account the previous results, a simple pseudo-phase diagram has been proposed for modified NBT ceramics, as shown in Fig. 5. This phase diagram can be constructed, from Fig. 3 and 4, to summarize the evolution of phases with the La^{3+} addition, see Fig. 5. This phase diagram evidences that the Curie temperature (T_C) increases monotonically and reaches the maximum of 350 °C at the highest La^{3+} content used in this study (x = 0.05), which corresponds to the tetragonal(antiferroelectric)-to-tetragonal(paraelectric) phase transition. On the other hand, the ferroelectric-to-antiferroelectric (T_{R-T}) phase transition decreases with the La^{3+} addition. It is also worth noting other characteristic aspects in the ceramic phase diagram with the highest La^{3+} content, since it has not been possible to detect the exact composition for which the ceramics become an antiferroelectric phase, see the fill pattern marked in Fig. 5. This behavior can be explained because the stability range of the tetragonal phase has increased to near room temperature at 5 at% of La^{3+}.

The piezoelectric constant d_{33} was measured as a function of temperature and the results are shown in Fig. 6. For NBT,

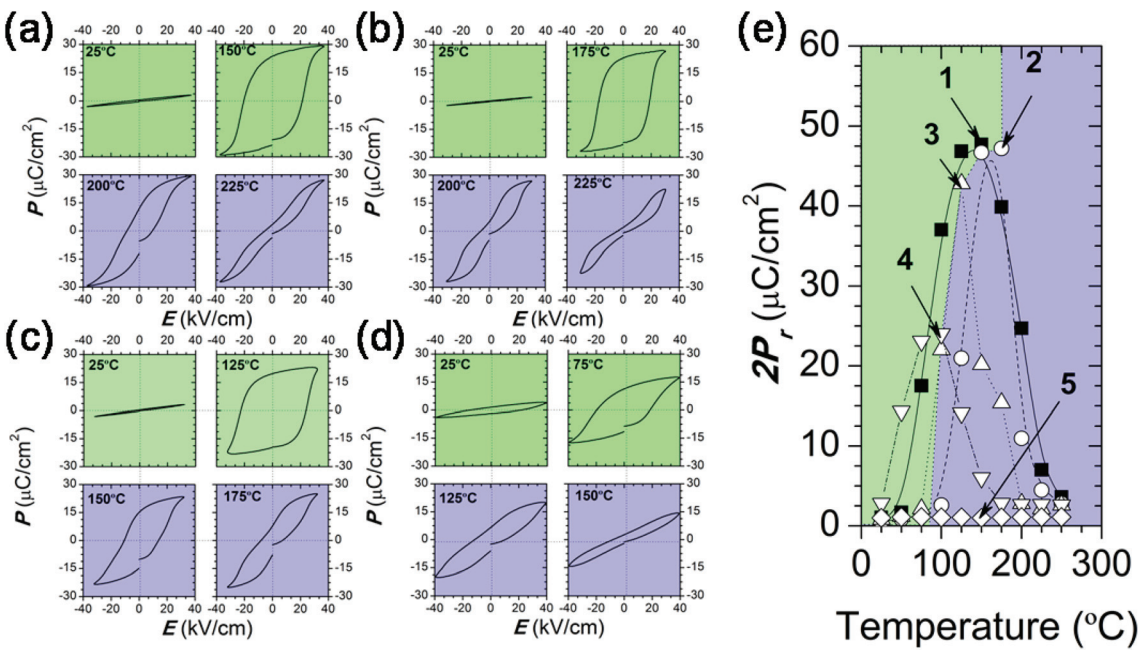

Fig. 4 Ferroelectric loops at different temperatures of (a) NBT, (b) NPBT; NPBLT, (c) x = 0.01, and (d) x = 0.03. (e) shows the evolution of $2P_r$ on NBT, NPBT and NPBLT systems as a function of temperature. The green color depicts the ferroelectric region, while the blue color delimits the anti-ferroelectric region of the system. The ceramic compositions represented in (e) are the same as in Fig. 3.

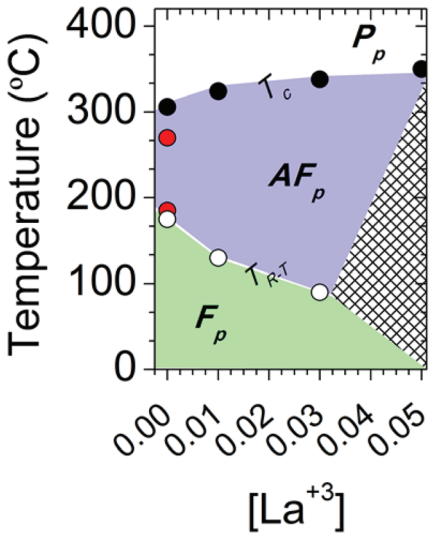

Fig. 5 Evolution of the T_C and rhombohedral to tetragonal phase (T_{R-T}) transition temperatures for ceramics with different La^{3+} content. Red dots represent the undoped ceramics, $Na_{0.5}Bi_{0.5}TiO_3$, while the black points in $x = 0.00$ depict the $Na_{0.5}Pr_{0.003}Bi_{0.497}TiO_3$ ceramics. The different electrical behaviors of the system are represented by a color code: green: ferroelectric phase (**F_p**); blue: anti-ferroelectric phase (**AF_p**); white: paraelectric phase (**P_p**); filled pattern: unknown phase, determined from dielectric and ferroelectric loop measurements.

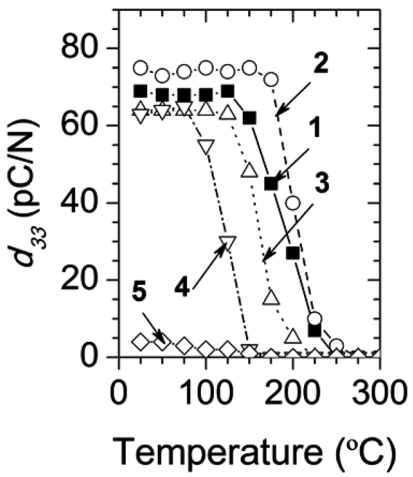

Fig. 6 Evolution of the piezoelectric constant, d_{33}, with the temperature in the NBT, NPBT; NPBLT systems. The ceramic compositions represented in Fig. 6 are similar to those in Fig. 3. Standard tolerance: piezoelectric constant ± 5%.

d_{33} is close to 70 pC N^{-1} at room temperature and remains constant until 150 °C; then it begins to decrease almost linearly till 225 °C and finally vanishes at 250 °C. Although the amount of Pr^{3+} is low, the effect on the piezoelectric properties is evident. First, d_{33} is slightly higher (75 pC N^{-1}) than in NBT, second, it is seen that d_{33} is nearly constant till 190 °C when it starts to decrease in the same manner as NBT, and it depolarizes at the same temperature. Then, the d_{33} stability slightly increases with a small amount of Pr^{3+}. The bismuth ion (Bi^{3+}) has an ionic radius of 1.17 Å with VIII coordination; the Pr^{3+} ion has an ionic radius of 1.126 Å with similar coordination.[18] Even though the ionic size is similar and they occupy the same crystallographic site (the A site in the perovskite structure), the electronic configuration of bismuth has the valence electrons in the 6*p* orbital, while praseodymium has its valence electrons in the 4*f* orbital. Then, probably the interaction between the Pr^{3+} 6*s* orbitals and the oxygen 2*p* orbitals favored the piezoelectricity as reported in the PZT.[15]

In contrast to Pr^{3+}, La^{3+} has decreased the piezoelectric properties of NBT, and also the stability of the ferroelectric phase, even though the ionic radius of La^{3+} is 1.16, which is close to that of Bi^{3+}. The results demonstrate that La^{3+} stabilizes the tetragonal structure, increasing the symmetry and modifying the oxygen octahedral tilting. The tetragonal structure has an $a^0a^0c^+$ tilt system compared with the rhombohedral which is $a^-a^-a^-$.[5] Then, A site coordination number changes from IX to VIII in these tilt systems.[19] Therefore, the lattice becomes more symmetric as the La^{3+} content increases, modifying the T_{R-T} and the ferroelectric and piezoelectric properties as well.

In Fig. 7, emission spectra (λ_{exc} = 350 and λ_{exc} 450 nm) are shown for the samples BNPT and BNPLT ($x = 0.03$ and 0.05). All the spectra are dominated by the red emission ascribed to the $^1D_2$–$^3H_4$ transition of Pr^{3+} at around 610 nm. These results are in agreement with recent reports.[10,11,20] Some differences are seen when exciting through the host (350 nm) or *via* the $^3P_2$ *f*-*f* transition at 450 nm (inset Fig. 7). In the latter case the relative contribution of transitions from $^3P_0$ to lower levels of Pr^{3+} is negligible compared with the former which present maxima at 496 nm ($^3P_0$–$^3H_4$); at 537 nm ($^3P_0$–$^3H_5$); at 656 nm ($^3P_0$–$^3F_2$); at 747 nm ($^3P_0$–$^3F_4$); the transition $^3P_0$–$^3F_3$ is overlapped with the transition $^1D_2$–$^3H_5$ which dominates the response at 700 nm, making it impossible to assign a maximum to that one. Fig. 8 shows the excitation spectra

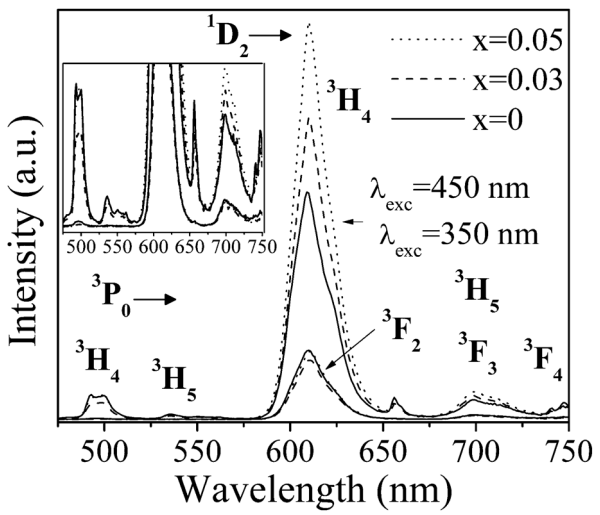

Fig. 7 Emission spectra of NPBT ($x = 0$) and NPBLT ($x = 0.03$ and $x = 0.05$), for excitation at 350 nm (bottom) and 450 nm (top). Emission spectra were recorded under identical conditions and were corrected for the wavelength dependent response of the detector system.

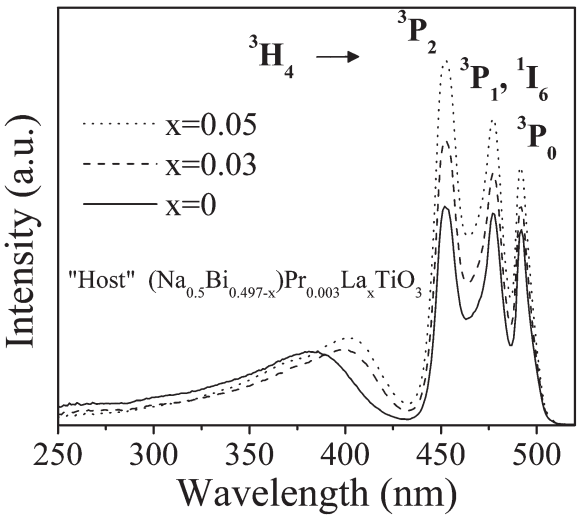

Fig. 8 Excitation spectra of NPBT (x = 0) and NPBLT (x = 0.03 and x = 0.05) monitoring emission at 610 nm. Excitation spectra were recorded under identical conditions and were corrected for the wavelength dependent intensity of the Xe lamp through a Si photodiode reference.

(λ_{em} = 610) for the samples BNPT and BNPLT (x = 0.03 and 0.05). All of them present a broad band in the UV as well as the *f–f* transitions of Pr^{3+} at 452 nm ($^3H_4$–$^3P_2$); at 477 nm ($^3H_4$–$^3P_1$, $^1I_6$); and at 492 nm ($^3H_4$–$^3P_0$). The noticeable effects of the La^{3+} addition are the shift in the excitation band in the low energy edge towards red (observed in Fig. 8), and the increase in the red emission which has not been reported in previous work. In the context of the low-lying Pr^{3+}-to-Ti^{4+} intervalence charge transfer (IVCT) state, the shift in the excitation band can be explained as follows. An empirical equation to estimate the position of IVCT is

$$\mathrm{IVCT}(Pr^{3+},\ cm^{-1}) = 58\,800 - \frac{10\,209}{d(Pr^{3+} - Ti^{4+})}$$

where $d(Pr^{3+}$–$Ti^{4+})$, expressed in nm, is the shortest distance separating these ions in the cell.[21] In general, the interionic distances among ions change as lanthanum is incorporated into the solid solution, due to the fact that the ionic radius of La^{3+} and that of Bi^{3+} differ slightly. In accordance with the previous equation, a red shift in the position of the IVCT implies that the distance between Ti^{4+} and Pr^{3+} (which is assumed to replace Bi^{3+} in the unit cell) should reduce its value. Interionic distances calculated from high resolution X-ray diffraction data reported recently in La-modified NBT, shown in Table 1, seem to support this fact.[22] Although in the samples with low La^{3+} concentrations (0.5 to 1.5 at%) the shortest distance $La^{3+}(Bi^{3+})$–Ti^{4+} tends to increase, for the sample with 2.0 at% concentration a reduction is observed in concordance with the results shown here and the IVCT model state.

The increase in the red emission is more difficult to elucidate. On the one hand the increase is probably due to the red shift in the IVCT. It is known that the emission properties of Pr^{3+} in NBT are mostly defined by the energy position of the IVCT state: the lower the IVCT state, the more efficient the

Table 1 Shortest $La^{3+}(Bi^{3+})$–Ti^{4+} distances as a function of La^{3+} concentration in at% (adapted from ref. 22)

La^{3+} concentration [at%]	Distance $La^{3+}(Bi^{3+})$–Ti^{4+} (nm)
0.0	0.31962(50)
0.5	0.32140(55)
1.0	0.32164(55)
1.5	0.32214(62)
2.0	0.31824(55)

quenching of the $^3P_0$ emission.[21] However, the emission spectra shown in the inset of Fig. 7 do not confirm this behaviour. The intensities of the emission transitions $^3P_0 \rightarrow {}^{2S+1}L_J$ for the samples with x = 0 and x = 0.05 are similar despite the shift in the excitation spectra. A systematic increase is observed only for the emission involving transitions from $^1D_2$ to $^3H_4$ and $^3H_5$. In order to clarify this increment, we have performed additional experiments. According to some reports,[23,24] the addition of lanthanides to oxides containing Bi^{3+} improves the crystallinity and reduces the oxygen vacancies. In our case this can be thought of as less quenching centers of luminescence by point defects in the material. Two evidences support this fact: the absorption band tail modification and the increase of the lifetimes due to La^{3+} addition. Fig. 9 shows the absorption spectra. The broad and intense band at wavelengths between 250 and 400 nm corresponds to the host absorption, the weak maxima observed at 452, 479, 492 and 600 nm are ascribed to transitions $^3H_4 \rightarrow {}^3P_2$, ($^3P_1$ $^1I_6$), $^3P_0$ and $^1D_2$ of Pr^{3+}, respectively. At first glance all spectra are similar, but if the absorption edge is observed in more detail (inset Fig. 9) it is clear that there is a modification in the absorption band tails. It is well known that in semiconductors a deviation from stoichiometry generates donors or acceptors depending on whether it is the cation, the anion or the vacancy which is in excess.[25] An oxygen vacancy deprives the crystal of one electron per broken bond and this makes the vacancy an acceptor. The acceptor level is localized around the

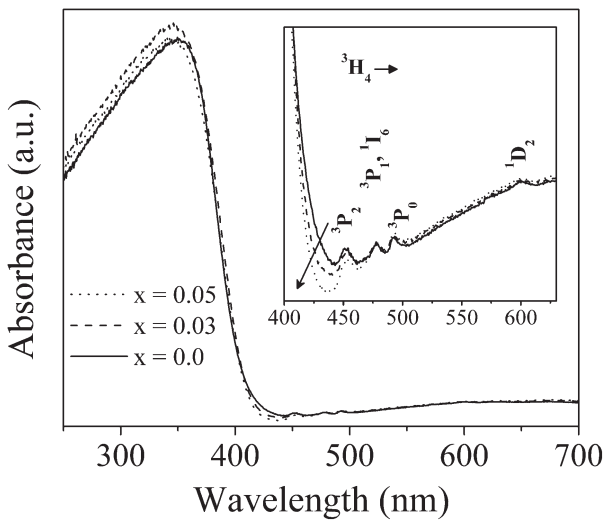

Fig. 9 Absorption spectra of NPBT (x = 0) and NPBLT (x = 0.03 and x = 0.05).

valence band, and therefore the oxygen vacancies produce a perturbation of the energy gap by the formation of tails of states extending the bands into the energy band gap, *i.e.*, at the edge of the absorption band. Thus the narrowing in the tails of the absorption edge (inset Fig. 9) provides evidence for the reduction of oxygen vacancies formation as the amount of La^{3+} increases. Concerning the lifetime of the transition $^1D_2 \rightarrow {}^3H_4$, an increase from 64 μs for the sample with $x = 0$ to 70 μs for the samples with $x = 0.03$ and $x = 0.05$ is observed; this result also supports the idea of the elimination of crystal defects and consequently the improvement in the emission of the samples containing La^{3+}.

Conclusions

In summary, we have found that the Pechini method reduces the temperature, and the synthesis time of the modified NBT system. This preparation method allows us to obtain a perovskite-phase without traces of secondary phases. The dielectric properties reveal a T_{R-T} anomaly near 190 °C for pure NBT, corresponding to antiferroelectric phase formation. This antiferroelectric phase can be confirmed through the ferroelectric loop measurements.

Furthermore, the dielectric, ferroelectric and optical properties of the modified NBT system can be easily controlled through rare earth cation doping. The addition of La^{3+} decreases the phase transition temperature, affecting the ferroelectric and piezoelectric properties. A decrease of the piezoelectric coefficient is observed with the increase of La^{3+} content, and all these properties disappeared for La^{3+} addition higher than 5 at%. This reduction is probably related to the stabilization of the paraelectric phase. However, La-doping does not modify drastically the P_r, while E_c decreases.

On the other hand, the red luminescence ascribed to the $^1D_2$–$^3H_4$ transition of Pr^{3+} is enhanced as the amount of La^{3+} is increased. This enhancement is due to the reduction in the oxygen vacancies. The reduction in the interionic distance between Ti^{4+}–Pr^{3+} produces a red shift in the IVCT excitation band in accordance with the IVCT model. The improvement in the red emission makes La^{3+}/Pr^{3+} co-doped NBT a promising material with interesting luminescent properties.

Acknowledgements

The authors want to thank CONACyT-México for providing financial support under projects CB-2010-01 154962 and CB-2011-01 166108, and MICINN (project MAT 2010-21088-C03-01). Also special thanks to Coordinación de la Investigación Cientifica-UNAM for providing a postdoctoral scholarship to R. López-Juárez and support under project number PAPIIT IT115011. Dr F. Rubio-Marcos is also indebted to CSIC for a "Junta de Ampliación de Estudios" contract (ref. JAEDOC071).

References

1 R. López, F. González, M. P. Cruz and M. E. Villafuerte-Castrejon, *Mater. Res. Bull.*, 2011, **46**, 70–74.
2 P. Setasuwon and S. Kijamnajsuk, *Sci. Technol. Adv. Mater.*, 2006, **7**, 780–784.
3 J. Wu, D. Xiao, W. Wu, Q. Chen, J. Zhu, Z. Yang and J. Wang, *J. Eur. Ceram. Soc.*, 2012, **32**, 891–898.
4 Y. Lin, C.-W. Nan, J. Wang, G. Liu, J. Wu and N. Cai, *J. Am. Ceram. Soc.*, 2004, **87**, 742–745.
5 G. O. Jones and P. A. Thomas, *Acta Crystallogr., Sect. B: Struct. Sci.*, 2002, **58**, 168–178.
6 E. Aksel, J. S. Forrester, J. L. Jones, P. A. Thomas, K. Page and M. R. Suchomel, *Appl. Phys. Lett.*, 2011, **98**, 152901.
7 J.-Y. Yi and J.-K. Lee, *J. Phys. D: Appl. Phys.*, 2011, **44**, 415302.
8 Y. Hou, M. Zhu, L. Hou, J. Liu, J. Tang, H. Wang and H. Yan, *J. Cryst. Growth*, 2005, **273**, 500–503.
9 T. Lu, J. Dai, J. Tian, W. Song, X. Liu, L. Lai, H. Chu, X. Huang and X. Liu, *J. Alloys. Compd.*, 2010, **490**, 232–235.
10 H. Zhou, X. Liu, N. Qin and D. Bao, *J. Appl. Phys.*, 2011, **110**, 034102.
11 P. Boutinaud, E. Cavalli, R. Velchuri and M. Vithal, *J. Phys.: Condens. Matter*, 2012, **24**, 075502.
12 S. Sakka, *Handbook of Sol–Gel Science and Technology. Processing, Characterization and Applications*, Kluwer Academic Publishers, pp. 60–69.
13 A. Z. Simões, C. Quinelato, A. Ries, B. D. Stojanovic, E. Longo and J. A. Varela, *Mater. Chem. Phys.*, 2006, **98**, 481–485.
14 H. Guo and Y. Qiao, *Appl. Surf. Sci.*, 2008, **254**, 1961–1965.
15 R. E. Cohen, *Nature*, 1992, **358**, 136–138.
16 H. Nagata, M. Yoshida, Y. Makiuchi and T. Takenaka, *Jpn. J. Appl. Phys.*, 2003, **42**, 7401–7403.
17 V. Dorcet, G. Trolliard and P. Boullay, *Chem. Mater.*, 2008, **20**, 5061–5073.
18 R. D. Shannon, *Acta Crystallogr., Sect. A: Cryst. Phys., Diffr., Theor. Gen. Cryst.*, 1976, **32**, 751–767.
19 P. M. Woodward, *Acta Crystallogr., Sect. B: Struct. Sci.*, 1997, **53**, 44–66.
20 H. Sun, D. Peng, X. Wang, M. Tang, Q. Zhang and X. Yao, *J. Appl. Phys.*, 2011, **110**, 016102.
21 P. Boutinaud, E. Cavalli and M. Bettinelli, *J. Phys.: Condens. Matter*, 2007, **19**, 386230.
22 E. Aksel, J. S. Forrester, H. M. Foronda, R. Dittmer, D. Damjanovic and J. L. Jones, *J. Appl. Phys.*, 2012, **112**, 054111.
23 H. Zhou, G. Wu, N. Qin and D. Bao, *J. Am. Ceram. Soc.*, 2010, **93**, 2109–2112.
24 H. Zhang, H. Yan and M.-J. Reece, *J. Appl. Phys.*, 2009, **106**, 044106.
25 J. I. Pankove, *Optical Processes in Semiconductors*, Dover Publications, Inc., New York, 1975, pp. 8–10.